JOURNAL OF MATERIALS SCIENCE 35 (2000) 4507–4518

Microstructural evolution during the supersolidus liquid phase sintering of nickel-based prealloyed powder mixtures

A. LAL*, R. G. IACOCCA, R. M. GERMAN
P/M Lab, 118 Research West, The Pennsylvania State University, University Park, PA 16802-6809, USA

A novel concept for full-density sintering is described. Two prealloyed powders with slight compositional differences are tailored to separate the solidus temperatures into high-melt and low-melt compositions. A mixture of these two powder compositions allows full-density sintering at a temperature between the two solidus temperatures. For these experiments, the two powders were nickel-based alloys, where the low-melt powder contained boron. The mixed powders were sintered at temperatures above the solidus of the low-melt powder to form a transient liquid that promoted rapid densification of the mixture. Microstructure evolution during sintering was assisted using quenching experiments. Variables in this study included the heating rate, peak temperature, hold time, and powder ratio. Interdiffusion between the two powders controls microstructure evolution, with a dominant role associated with boron diffusion and reaction. The transient liquid phase responsible for densification is linked to boron diffusion and subsequent compound precipitation.

1. Introduction

Supersolidus liquid phase sintering (SLPS) allows for the densification of a prealloyed powder between the solidus and liquidus temperatures [1–18]. It differs from classic liquid phase sintering which starts with mixed elemental powders, which are heated into a two phase solid-liquid temperature range to induce densification [3–8]. As a variant on supersolidus liquid phase sintering, densification of prealloyed powders can be enhanced by additives which form a low temperature liquid [14–18]. Further, supersolidus liquid phase sintering is possible using mixtures of two prealloyed powders [2]. This process is the most complex variant of SLPS, yet proves useful in high alloy systems.

Tandon and German [2] investigated the processing parameters in the densification of mixed nickel-based superalloy powders. One powder was doped with boron to lower the melting temperature range by formation of the Ni-B eutectic. In this system, the low-melt powder forms a liquid that densifies the mixed powder structure. A homogeneous product is achieved during sintering by interdiffusion between of the constituent powders. Densification is controlled through the powder mixture, where a higher proportion of low-melt powder gives more liquid and accelerates densification. Alternatively, an increase in the high-melt powder fraction broadens the temperature range over which densification occurs.

One advantage of mixed prealloyed powders is the fabrication of dense, homogeneous structural components without distortion [1]. Success with this variant relies on a small proportion of the low-melt powder. Alternatively, the two powder concept can be used to form a brazing mixture by increasing the proportion of low-melt powder [19–23]. In each case, the powder composition is selected to tailor the final properties and rheological behavior during sintering.

German [1] has created a model for SLPS that assumes viscous flow densification driven by capillary forces acting on the partially dense semisolid structure. To apply this model to densification of prealloyed powder mixtures requires knowledge of microstructure development concomitant with densification. Controlling features are the liquid content and distribution as functions of temperature and time during sintering. Further, in the nickel-base alloys investigated here, the precipitation, borides reduces the liquid volume over time. This paper builds on recent work [24] to enable application of SLPS models to prealloyed powder mixtures.

2. Experimental procedures

Gas atomized nickel-based powders were employed for the low-melt (LM) and high-melt (HM) powders. Compositions for the two powders are given in Table I and scanning electron micrographs are shown in Figs 1 and 2. Table II summarizes the powder characteristics. The particle size distribution is given in terms of the particle sizes at the 10, 50, and 90 percentage

* Now with Motorola, Ft. Lauderdale, FL, USA.

TABLE I Chemical composition of the powders in weight percent

Powder	Ni	Co	Cr	Al	Ti	B	Ta	W	Mo	Zr
LM	55.5	24.3	15.1	1.2	-	2.7	1.2	-	-	-
HM	60.4	9.5	14.0	3.0	5.0	-	-	4.0	4.0	0.1

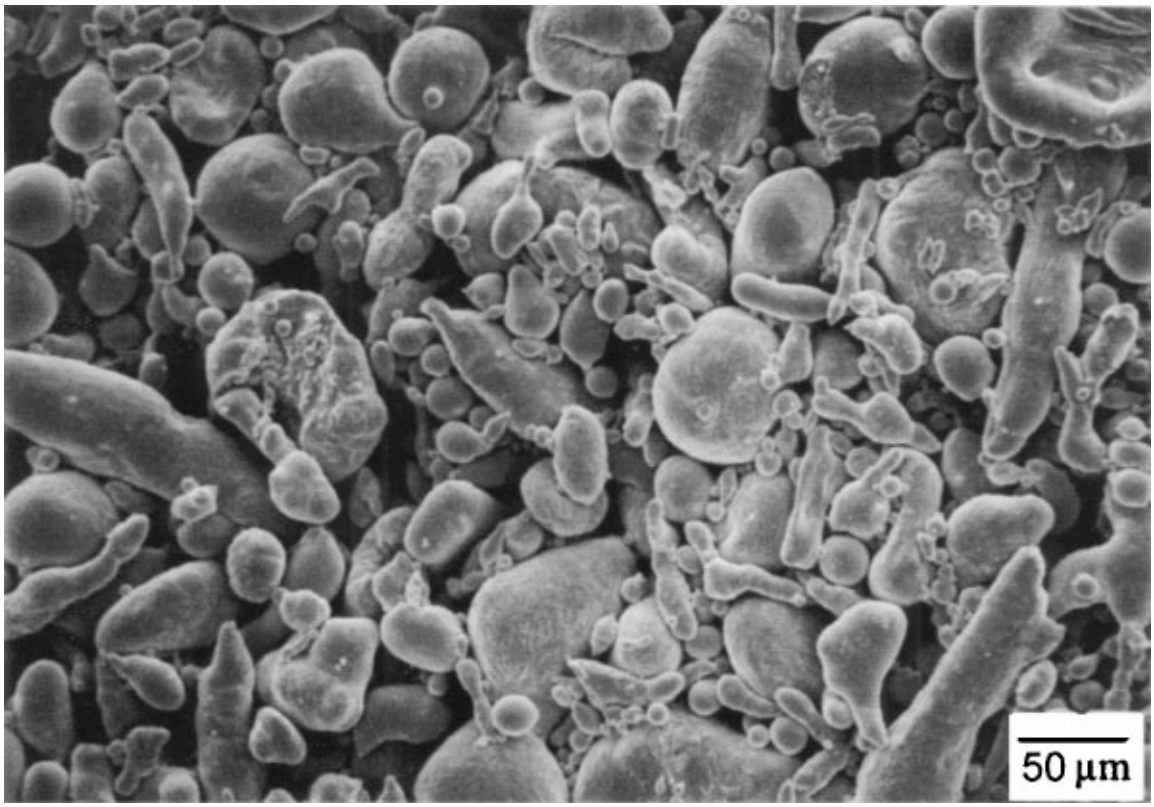

Figure 1 Scanning electron micrograph of gas atomized LM powder.

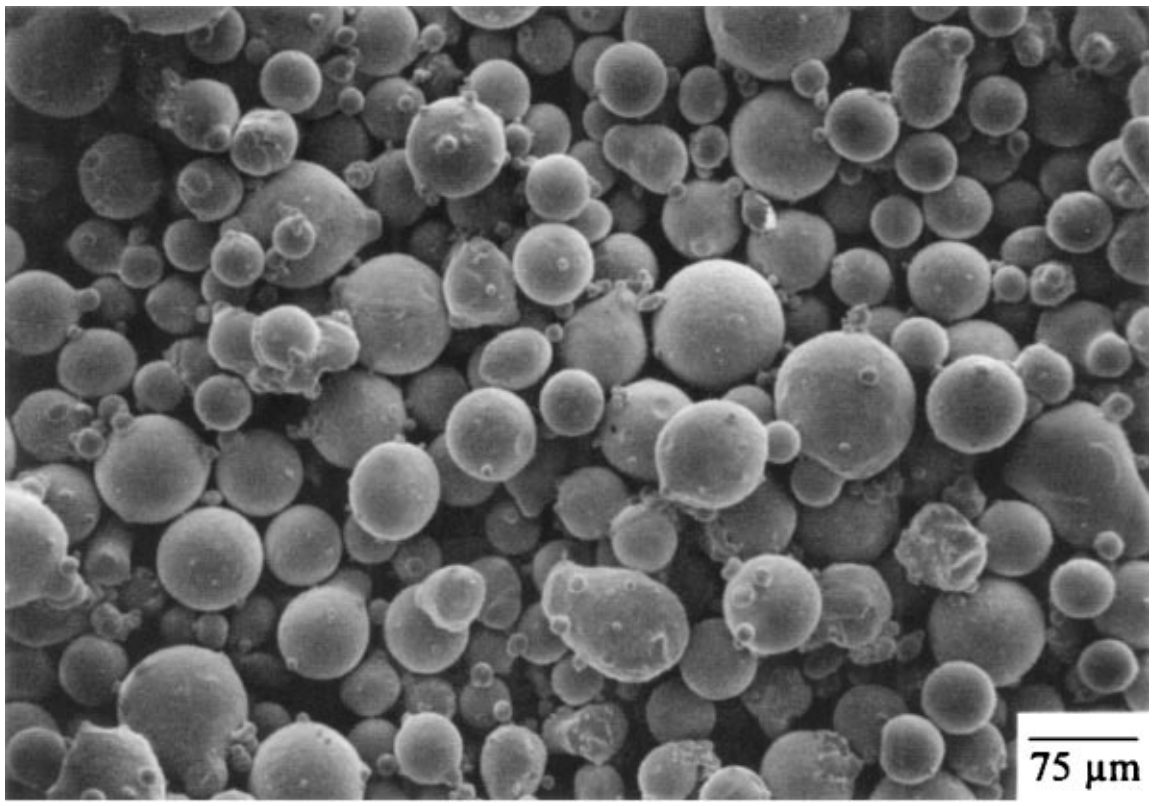

Figure 2 Scanning electron micrograph of gas atomized HM powder.

TABLE II Powder characteristics

Powder Characteristics	LM Powder	HM Powder
Apparent Density, (g/cm^3)	4.6	4.8
Tap Density, (g/cm^3)	5.6	5.3
Pycnometer Density, (g/cm^3)	8.1	8.1
Size Distribution, (μm)		
D_{10}	18	57
D_{50}	53	88
D_{90}	116	133
Internal Microstructure	Dendritic	Dendritic
Solidus Temperature, °C	1060	1285
Liquidus Temperature, °C	1089	1330

TABLE III Compositions and heating cycles of samples

Sample Number	Composition and Heating Cycle
1	100% LM powder, quenched at 1085°C after a 15 min hold
2	50-50 wt.% mixture of LM and HM powders, quenched after 60 min at 1080°C
3	50-50 wt.% mixture of LM and HM powders, quenched from 1145°C without any hold
4	50-50 wt.% mixture of LM and HM powders, quenched after a 20 min hold at 1145°C
5	50-50 wt.% mixture of LM and HM powders, quenched after a 60 min hold at 1145°C
6	50-50 wt.% mixture of LM and HM powders, sintered at 1145°C for 60 min and furnace cooled

points on the cumulative mass distribution. The solidus and liquidus temperatures were determined using differential thermal analysis, and are included in Table II.

Powder mixtures were prepared using 20 min mixing in a Turbula device. Both batch and interrupted sintering experiments were used to follow sintering. For the batch experiments, loose powder was vibrated into alumina crucibles and sintered in flowing hydrogen (dew point below −30°C) followed by furnace cooling to room temperature. Microstructure evolution was captured using interrupted cycles. A vertical water-quench furnace was employed with an estimated cooling rate of 10^3 °C/s. Heating was at 10°C/min for all experiments. The samples were analyzed by standard microscopy techniques.

Table III identifies the compositions and thermal cycles. Sample 1 provided information on liquid formation in the LM powder. Samples 2 through 5 consisted of 50-50 wt.% mixtures of the LM and HM powders, with selected quenching temperatures and hold times. These allowed identification of the phase evolution during sintering. Initially, a temperature of 1080°C was used since it is slightly below the liquidus of the LM powder. Subsequently, a higher temperature of 1145°C allowed for more liquid. Finally, the last sample was slow cooled using a 50-50 mixture to determine phase and composition changes during normal slow cooling.

3. Results

3.1. Sample 1 (100% LM, 10°C/min to 1085°C, 15 min hold, water quench)

This 100% LM powder sample provided information on the nucleation of the first liquid. A back scattered electron image of the cross-sectioned sample is shown in Fig. 3. The three distinct phases visible as light gray, dark gray, and black were identified as solid, liquid, and precipitate, respectively. Compositions for the phases are given in Table IV based on electron microprobe analysis. The major difference is in the segregation of B and Ta to the liquid phase. Since the peak temperature was above the solidus (1060°C), the boron-rich darker phase represents solidified liquid. Boron forms eutectic liquid in nickel-based and cobalt-based prealloyed powders [2, 23–27]. The small black regions

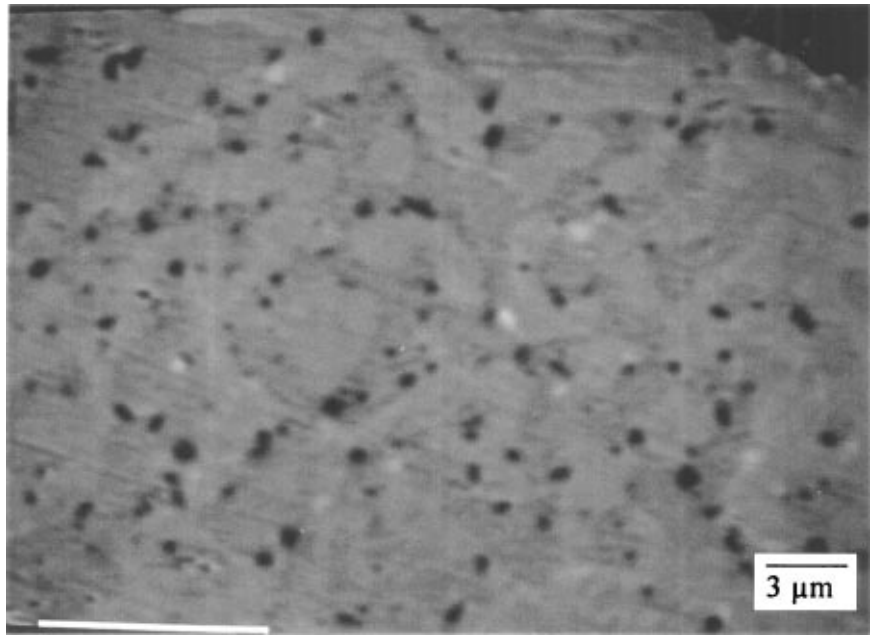

Figure 3 Backscattered electron image of the LM powder, water quenched from 1085°C after 15 min. The lighter gray and the relatively darker regions are the solid and liquid phases, respectively. The black precipitates are borides.

TABLE IV Composition of phases in LM powder quenched from 1085°C after 15 min (Sample 1)

Element	Solid	Liquid	Precipitate Region*
	at.%	at.%	at.%
Ni	55.8	50.9	7.4
Co	25.2	22.6	9.3
Cr	17.5	12.2	55.8
Al	1.5	1.5	0.2
Ti	0.0	0.0	0.0
B	0.0	12.4	27.3
Ta	0.0	0.4	0.0
W	0.0	0.0	0.0
Mo	0.0	0.0	0.0

*Note: Includes some of the surrounding phase.

correspond to Cr_2B precipitates in the liquid phase. The Ni and Co detected in the analysis is from electron beam stimulation of the surrounding matrix.

The quenched LM powder does not show the classic supersolidus liquid phase microstructure. Normally, liquid forms along grain boundaries, in isolated droplets in the grains, and at the particle contacts [27]. In the LM powder, which was originally dendritic, the dendrite arms pinched off once the liquid formed, leaving discrete solid grains separated by liquid [28].

Because the LM powder forms the initial liquid, the composition analysis in Table IV provided the means to identify liquid in subsequent quenched samples. As expected, liquid formation was consistently associated with high boron regions. Thus, in subsequent discussions, regions identified as liquid refer to the phase existing at the time of quenching.

3.2. Sample 2 (50-50 wt.% mixture, 10°C/min to 1080°C, 60 min hold, water quench)

A back scattered electron image of the microstructure is shown in Fig. 4. A large spherical HM particle is on the right and a LM irregular particle is in contact on the left. The LM particle is mostly solid, with isolated pockets of liquid (seen in relief). Dark precipitates are evident in the LM particle. The HM particle exhibits liquid formation near the neck region with extensive precipitate formation in the remainder. These precipitates were not found in the as-received powder. Further, the pure HM powder did not show these precipitates, even when quenched from 1145°C after 180 min. Table V lists the compositions of the solid, liquid, and precipitates in the LM particle, HM matrix (i.e., excluding precipitates), and HM precipitates. Further, the table gives the bulk composition of a HM particle after quenching. It can be compared to the composition of the initial HM powder, which is included in the table. The LM particle shows Ti, W, and Mo, which were not present in the initial composition. Further, the HM particle has 8.2 at.% (1.6 wt.%) boron, although no boron was present in the initial composition. The boron in the HM particles is present as boride precipitates. The HM particle matrix, like the solid LM matrix, is devoid of boron.

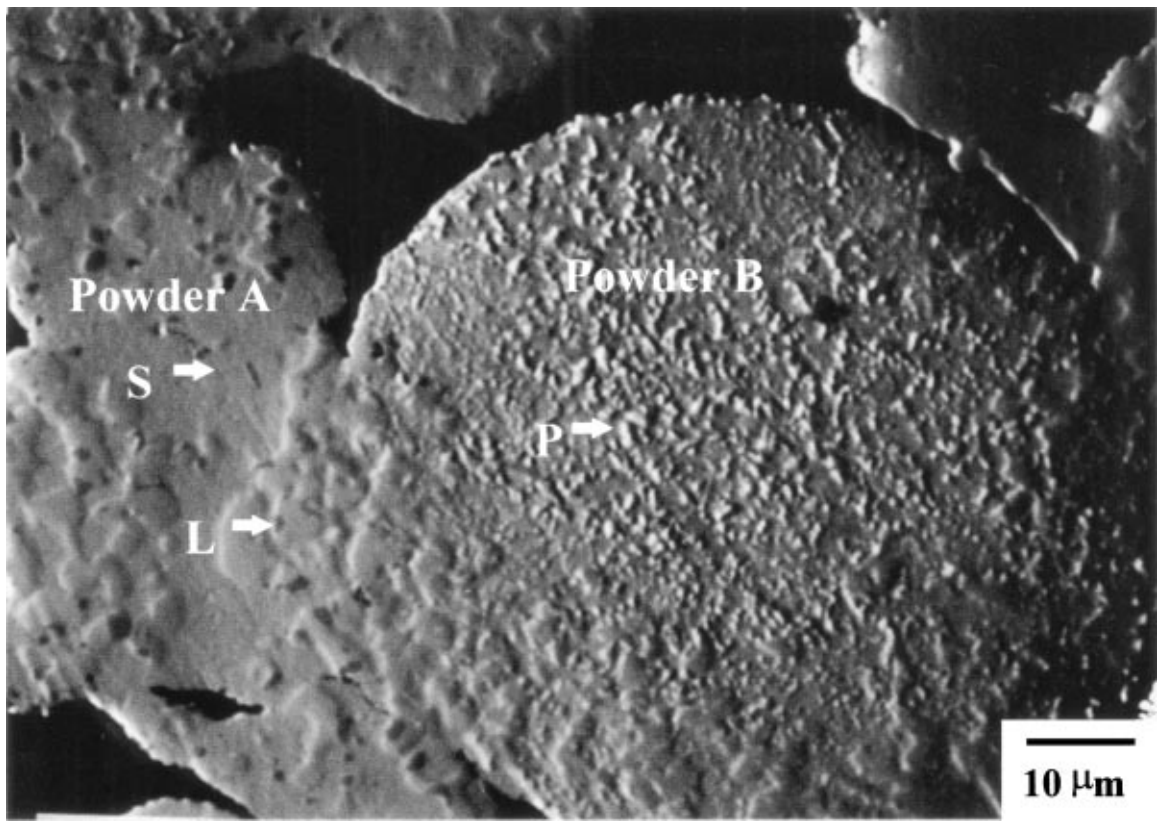

Figure 4 Backscattered electron image from a 50-50 wt.% powder mixture, quenched after 60 min at 1080°C (Sample 2). The HM particle shows precipitates (marked as "P"). The LM powder is partially molten and the solid and liquid regions are marked as "S" and "L", respectively. Liquid has formed in the HM particle at the neck region.

TABLE V Compositions of the phases present in a 50-50 wt.% mixture of powders quenched from 1080°C after a hold of 60 min (Sample 2). The original composition of HM powder is included for comparison

Element	Solid in LM	Liquid in LM	Precipitate in LM*	HM Powder Matrix	HM Powder Precipitates*	HM Powder (bulk)	Original HM Powder
	at.%	at.%	at.%	at.%	at.%	at.%	at.%
Ni	57.7	53.2	4.3	66.0	21.8	53.3	59.2
Co	23.0	17.8	8.0	12.4	5.9	8.5	9.3
Cr	17.0	7.0	55.3	12.3	30.4	15.9	15.5
Al	1.5	1.1	0.0	4.3	1.2	4.4	6.4
Ti	0.3	4.3	0.1	4.1	2.2	5.8	6.0
B	0.0	16.2	31.9	0.0	31.7	8.2	0.0
Ta	0.0	0.1	0.0	0.0	0.0	0.0	0.0
W	0.2	0.1	0.1	0.4	2.3	1.5	1.2
Mo	0.3	0.2	0.3	0.5	4.5	2.4	2.4

*Note: Includes some of the surrounding phase.

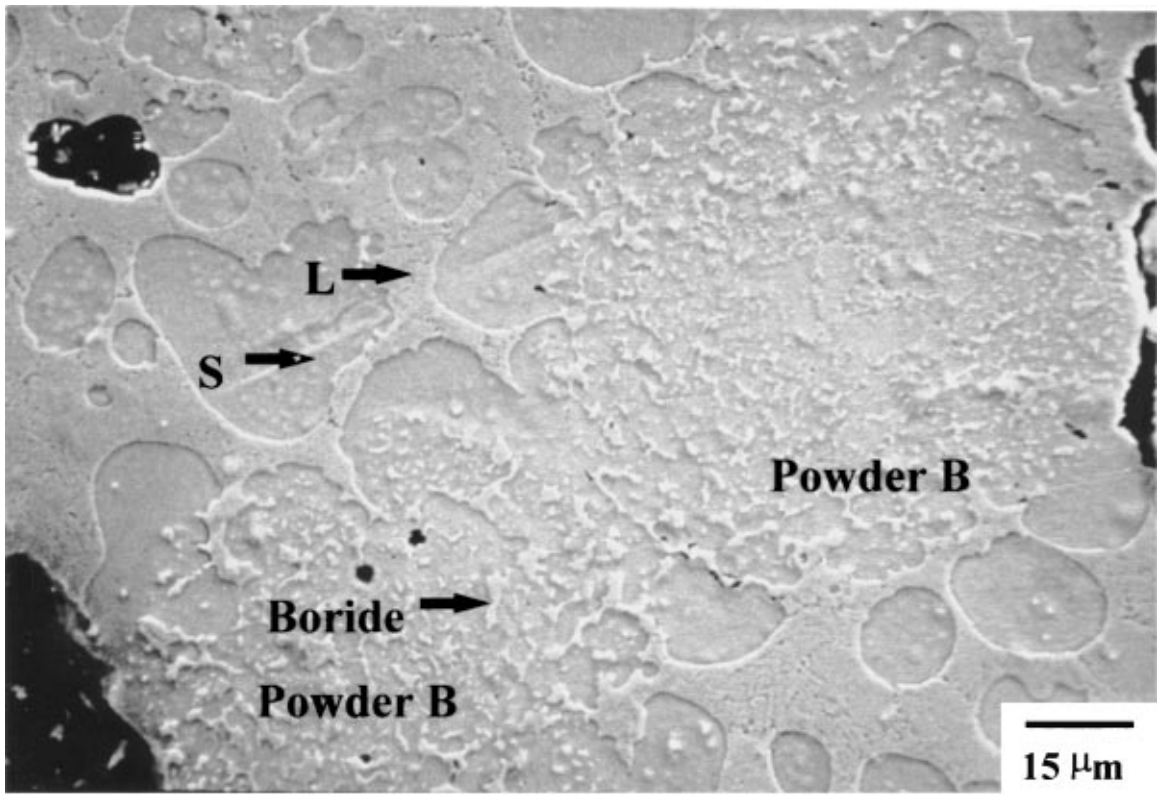

Figure 5 Scanning electron micrograph of a 50-50 wt.% powder mixture, quenched from 1145°C (without a hold) (Sample 3). The HM particles are surrounded by solid grains (S) and liquid (L) formed on melting of LM powder.

3.3. Sample 3 (50-50 wt.% mixture, 10°C/min to 1145°C, no hold, water quench)

By 1145°C there was significant densification and homogenization. Fig. 5 is a scanning electron micrograph of Sample 3 showing two HM particles in a matrix of liquid and solid grains formed by LM particle melting. Note the LM particle is not completely liquid even though the maximum temperature (1145°C) was over the liquidus temperature (1089°C). The HM particles show no evidence of liquid, but do have boride precipitates.

Phase compositions are listed in Table VI. They include the solid and liquid in the matrix, the precipitates present in the liquid and in the HM particles, and a HM particle as a whole. The solid and liquid phases that constitute the matrix exhibit Ti, W, and Mo, which were initially absent in the LM powder. Note that the composition of the solid is typical for nickel-based gamma alloys [29]. Further, analysis of a HM particle showed 6.8 at.% (1.3 wt.%) boron in the form of boride precipitates.†

Qualitative elemental mapping showed segregation among phases as shown in Fig. 6, supporting quantitative compositional analysis. The backscattered electron image on the top left has a HM particle surrounded

† The possibility these boride precipitates were not present at the sintering temperature and formed on cooling seems negligible. For that to happen the Ni-rich solid solution in the HM powder needs to have a high boron solubility at the sintering temperature. This is unlikely considering that Ni has a very low solubility for boron at high temperatures.

TABLE VI Composition of phases present in a 50-50 wt.% mixture of powders quenched from 1145°C (Sample 3). The original composition of HM powder is included for comparison

Element	Solid In Matrix	Liquid in Matrix	HM Powder	Original HM Powder	Precipitate in Liquid*	Precipitate in HM Powder*
	at.%	at.%	at.%	at.%	At.%	at.%
Ni	58.6	52.4	55.5	59.2	3.7	10.6
Co	20.1	18.0	11.7	9.3	5.5	6.8
Cr	15.1	13.3	15.1	15.5	54.9	39.6
Al	4.0	1.3	4.6	6.4	0.0	0.2
Ti	1.3	3.3	3.3	6.0	0.2	0.8
B	0.0	10.6	6.8	0.0	32.2	32.8
Ta	0.1	0.2	0.0	0.0	0.0	0.1
W	0.3	0.2	1.2	1.2	1.4	3.2
Mo	0.5	0.7	1.8	2.4	2.1	5.9

*Note: Includes some of the surrounding phase.

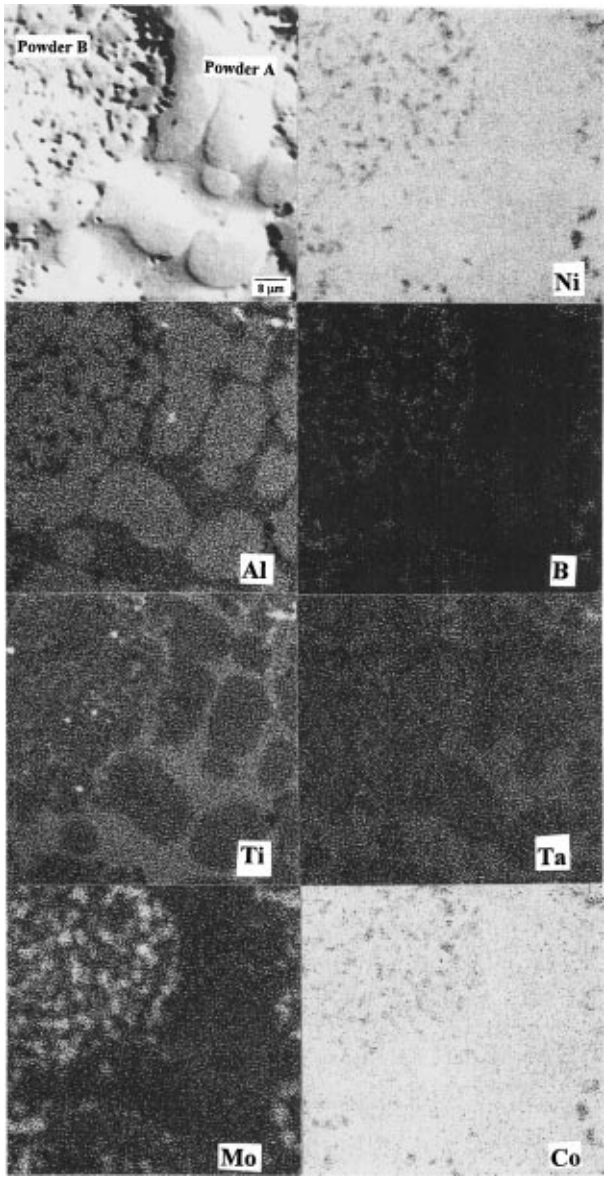

Figure 6 Electron microprobe elemental maps for a 50-50 wt.% powder mixture, quenched from 1145°C (without a hold) (Sample 3).

by a matrix of solid grains and liquid. Precipitates are apparent as dark phases in the HM particle and matrix. The corresponding elemental maps provide a visual comparison of the partitioning between phases. Brighter areas represent regions of high concentration of an element compared to darker areas. Considerable interdiffusion occurred between the HM particles and the partially melted LM particles. Elements present initially in only one of the powders are now evident in the other.

3.4. Sample 4 (50-50 wt.% mixture, 10°C/min to 1145°C, 20 min hold, water quench)

Sample 3 evidenced boron-rich precipitates and no liquid in the HM particles. However, Sample 4 showed that liquid formed in the HM particles over time. Fig. 7 is a back-scattered electron image of a HM particle in the quenched microstructure, showing both liquid and boride precipitates. The liquid has formed an interconnected structure, resulting in fragmentation of the HM particle.

3.5. Sample 5 (50-50 wt.% mixture, 10°C/min to 1145°C, 60 min hold, water quench)

Fig. 8 is an optical image of Sample 5 quenched after a long hold. Now the microstructure consists of coarsened grains with liquid at the grain boundaries. The microstructure is uniform and with no evidence of the original particles. Hence, a hold of 60 min was sufficient to homogenize the powder mixture. The micrographs show clusters of small blocky precipitates dispersed predominantly in the liquid phase. These precipitates appear to be clustered at prior HM particle sites.

Table VII gives the compositions of the solid, liquid, and precipitates. As before, boron segregates to either

TABLE VII Composition of phases present in a 50-50 wt.% mixture of powders quenched from 1145°C after a 60 min hold (Sample 5)

Element	Solid	Liquid	Precipitate*
	at.%	at.%	at.%
Ni	58.9	54.6	6.6
Co	18.3	17.5	5.9
Cr	15.4	11.4	43.9
Al	4.5	1.4	0.0
Ti	1.8	4.4	0.9
B	0.0	9.9	30.8
Ta	0.1	0.2	0.1
W	0.4	0.1	4.2
Mo	0.6	0.5	7.6

*Note: Includes some of the surrounding phase.

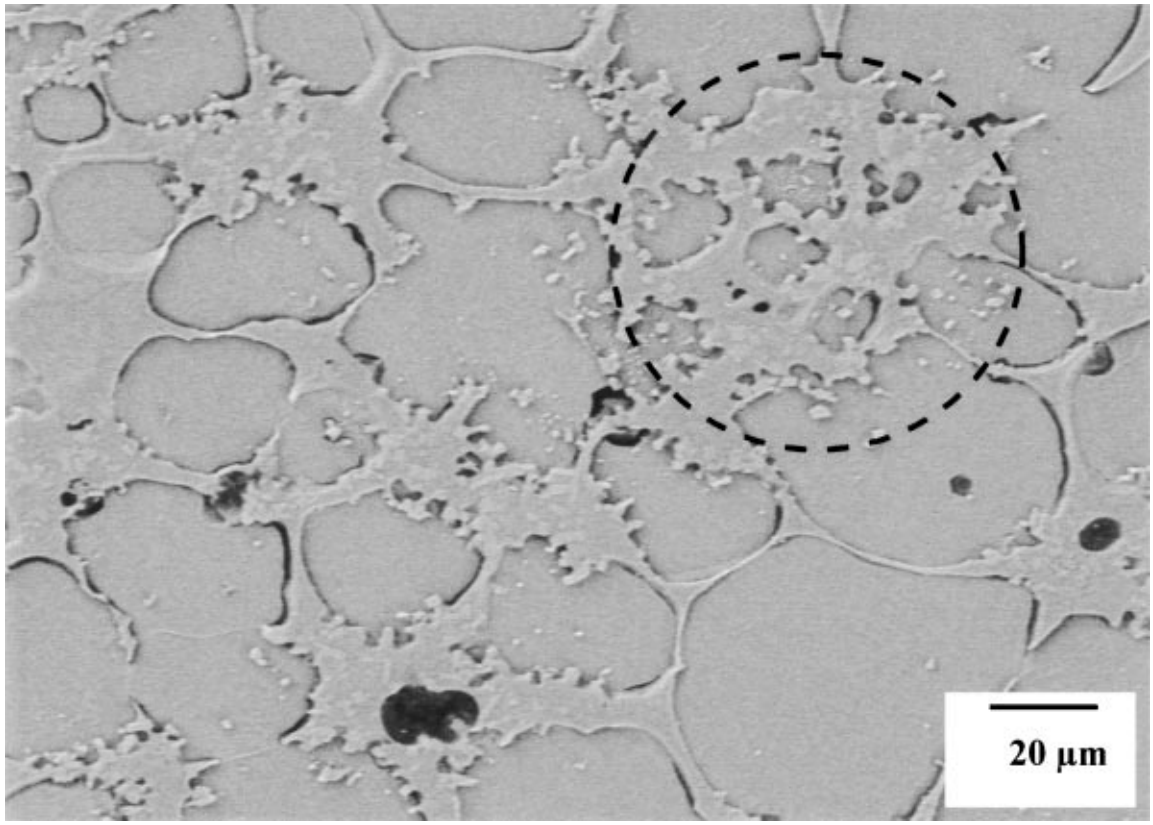

(a)

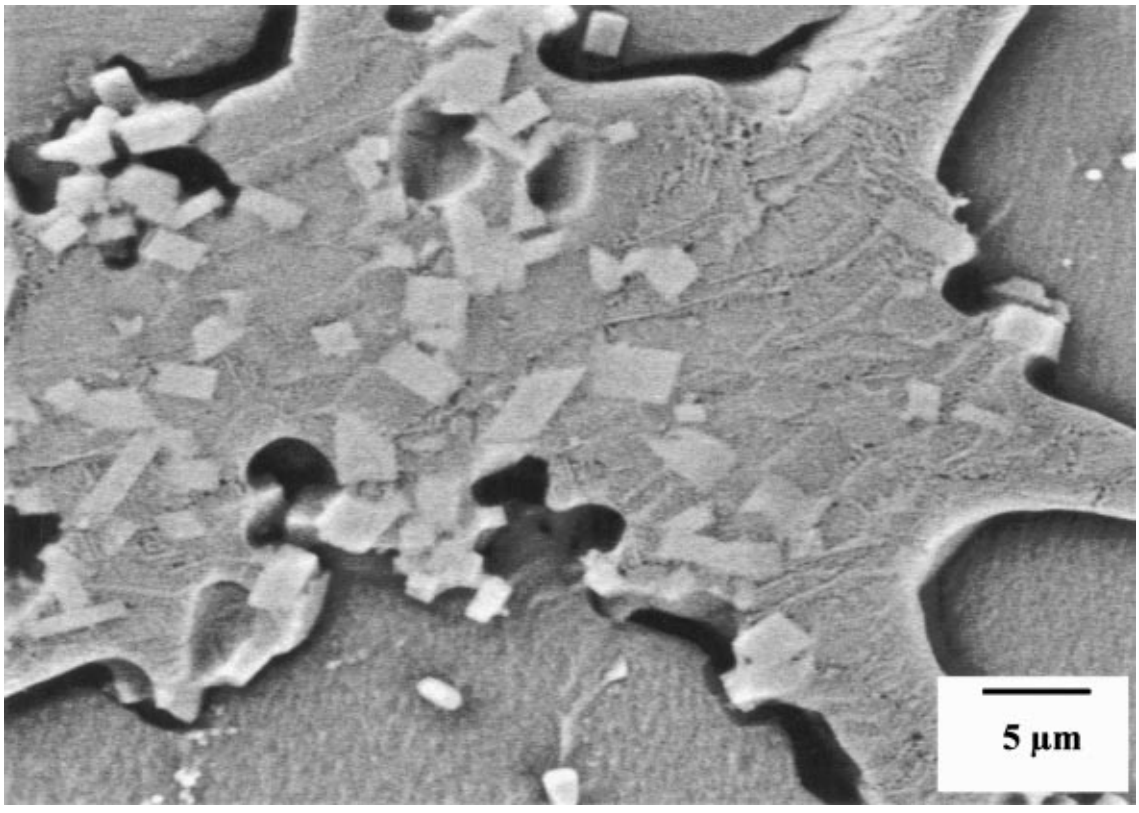

(b)

Figure 7 Optical micrograph of a 50-50 wt.% powder mixture, water quenched from 1145°C after a hold of 20 min (Sample 4), showing liquid in a HM particle.

the liquid or the precipitates. No traceable quantities of boron are present in the solid grains. The refractory elements, W and Mo, have segregated predominantly to the blocky precipitates along with B and Cr. The composition of these precipitates is similar to the composition of the HM powder precipitates observed after shorter times. Thus, they concentrate at the prior HM particle sites.

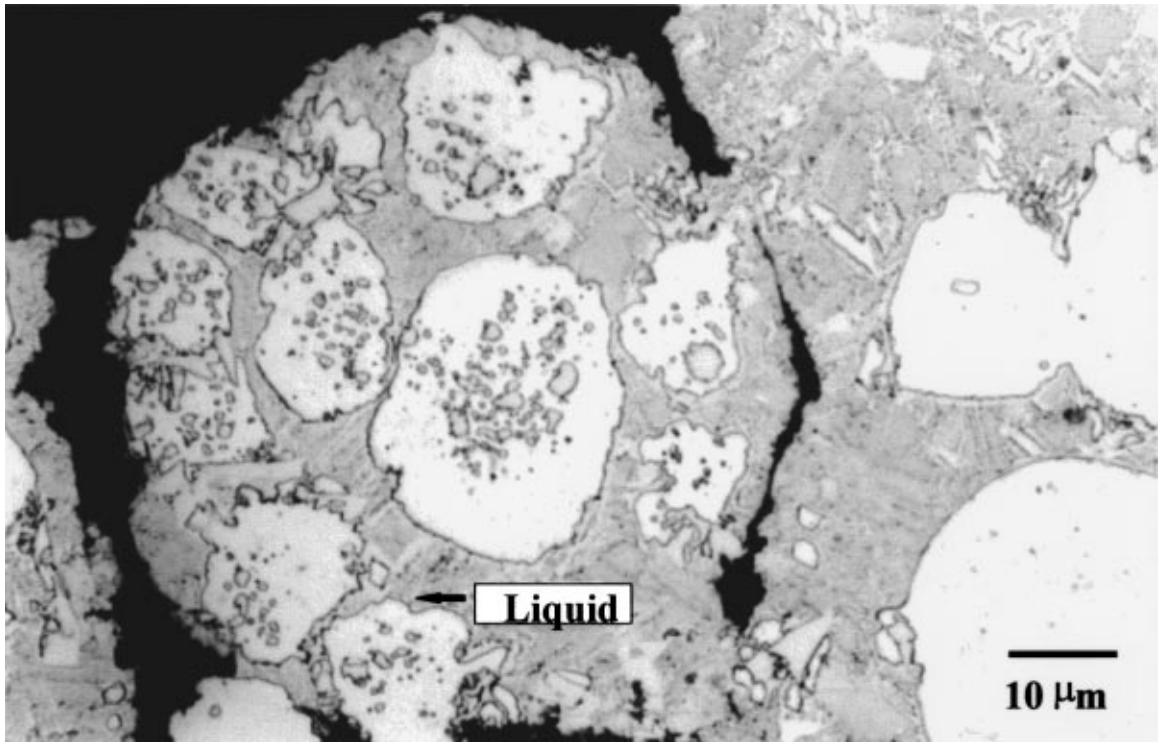

Figure 8 Backscattered electron images of a 50-50 wt.% powder mixture, quenched from 1145°C after a 60 min hold (Sample 5). Small blocky precipitates are clustered at prior HM particle sites, as marked by the dotted circle in (a) and shown at a higher magnification in (b).

3.6. Sample 6 (50-50 wt.% mixture, 10°C/min to 1145°C, 60 min hold, furnace cool)

Fig. 9 is a secondary electron and a backscattered electron image of Sample 6. The microstructure consists of grains with 'script' phase at the grain boundaries and blocky precipitates. The compositions of the three phases; the matrix, the script phase, and the blocky precipitates, are tabulated in Table VIII. The segregation of the elements to the three phases is similar to that seen in the Sample 5. This sintered sample differs from the quenched sample (Sample 5) in the presence of the script phase and the absence of liquid. A comparison of the compositions confirms that the liquid present at the processing temperature (observed in quenching) is the precursor of the script phase. The compositions are slightly different, because slow cooling allowed more interdiffusion. The initial packing density of the powder mixture was 56.5% of theoretical, whereas the final sintered density was 96% of theoretical.

TABLE VIII Composition of the phases present in a 50-50 wt.% mixture of powders sintered at 1145°C for 60 min (Sample 6)

Element	Matrix	Script Phase	Blocky Precipitate*
	at.%	at.%	at.%
Ni	59.6	54.0	7.6
Co	17.5	16.5	7.2
Cr	15.0	5.6	45.5
Al	4.8	0.7	0.0
Ti	2.0	6.5	1.1
B	0.0	16.3	32.1
Ta	0.1	0.1	0.0
W	0.4	0.1	1.2
Mo	0.6	0.2	5.3

*Note: Includes some of the surrounding phase.

During liquid phase sintering, component distortion is a concern. However, Sample 6 did not distort and only samples with the 50-50 wt.% powder mixtures sintered for 60 min at temperatures of 1165°C and higher lost shape.

4. Discussion

4.1. Microstructural evolution

Homogenization occurs simultaneously with densification for these mixed powders. The LM powder begins to melt above its solidus temperature of 1060°C. Boron diffusion out of the LM powder alters its melting behavior such that it is not completely liquid at temperatures much higher than its liquidus (1089°C). At temperatures slightly above the LM solidus, boron diffusion into HM particles precipitates borides rich in W, Mo, and Cr (as shown in Fig. 4). When the sintering temperature is higher (for example, 1145°C), boron diffusion forms liquid within the HM particles. In that case, the boride precipitates in the HM particles form during heating. The liquid fragments the HM particles. The spreading of a liquid film throughout the structure and the increased particle contact due to densification promotes homogenization.

Interdiffusion leads to compositional changes in the solid and liquid phases formed on the melting the LM particles. The composition of these phases moves toward the overall composition of the alloy mixture. Interdiffusion continues until no difference remains between LM powder and HM grains. Thus, the microstructure after about a 60 min hold at 1145°C consists of relatively coarse solid grains, dispersed in an interconnected liquid (Fig. 8). The boride precipitates that formed initially in the HM powder are stable, and once formed undergo minor compositional changes.

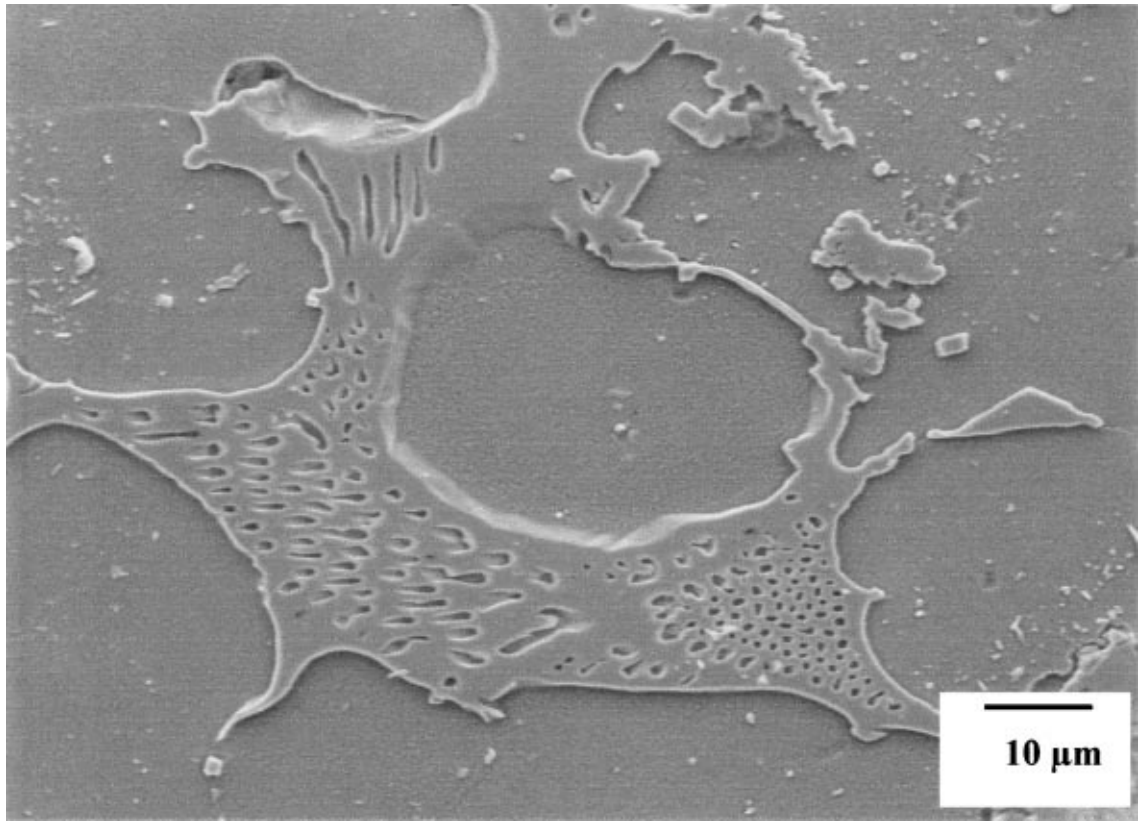

(a)

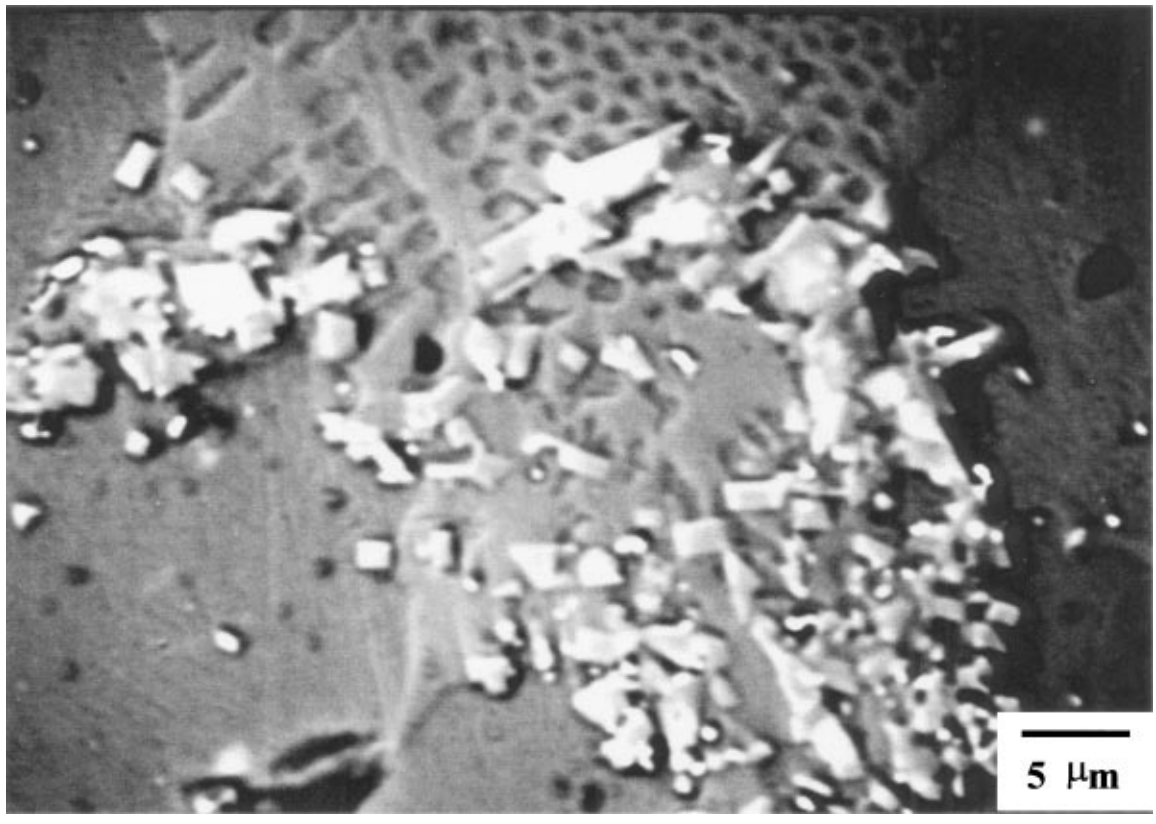

(b)

Figure 9 Scanning electron micrograph (a) and backscattered electron image (b) of a 50-50 wt.% powder mixture sintered at 1145°C for 60 min and furnace cooled (Sample 6). The script phase and blocky precipitates are evident.

Liquid at the sintering temperature precipitates a script phase on furnace cooling. This phase has been observed earlier for similar Ni-based alloy systems, and has been identified as a topologically closed packed phase [23].

To determine the effect of HM powder on the LM melting behavior, differential thermal analysis was performed on a homogenized 50-50 wt.% powder mixture (Sample 5). The solidus and liquidus temperatures were 1107 and 1230°C, respectively. These may be compared

to the lower values for LM powder. Hence, the melting characteristics of the LM powder change continuously with homogenization, approaching the solidus and liquidus temperatures corresponding to the overall composition.

In the presence of about 25 to 30 vol. % liquid, interdiffusion and homogenization are complete within one hour. However, insufficient temperature or time results in an inhomogeneous structure. In such microstructures, the HM powder is still distinguishable and contains some solidified liquid and boride precipitates. An example is shown in Fig. 10, which is an optical micrograph of a 50-50 wt.% mixture sintered at 1125°C for 60 min.

4.2. Mechanism of Interdiffusion

The mechanism by which homogenization occurs between the LM powder and the HM powder is sketched in Fig. 11. Hypothetical binary phase diagrams representing the two powders aid in describing boron diffusion and microstructural changes. The initial boron content is C_0 in the LM powder, and zero in the HM powder

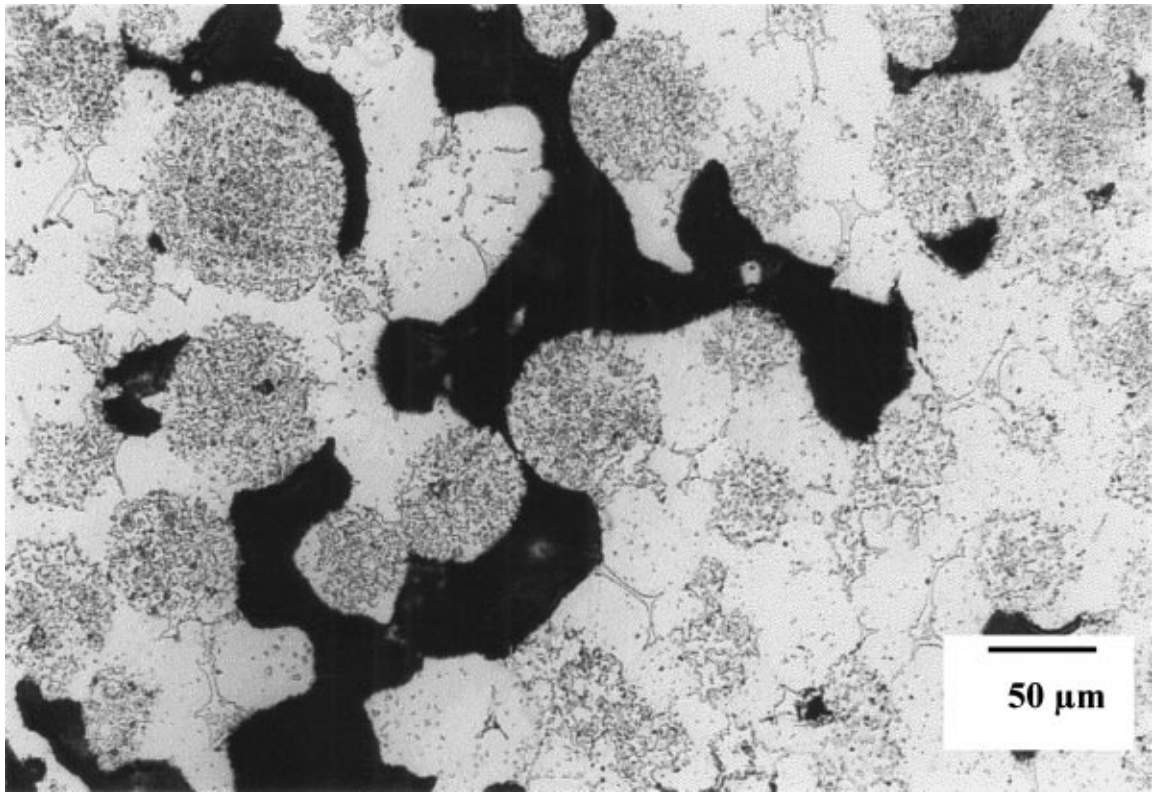

Figure 10 Optical micrograph of a 50-50 wt.% powder mixture sintered at 1125°C for 60 min.

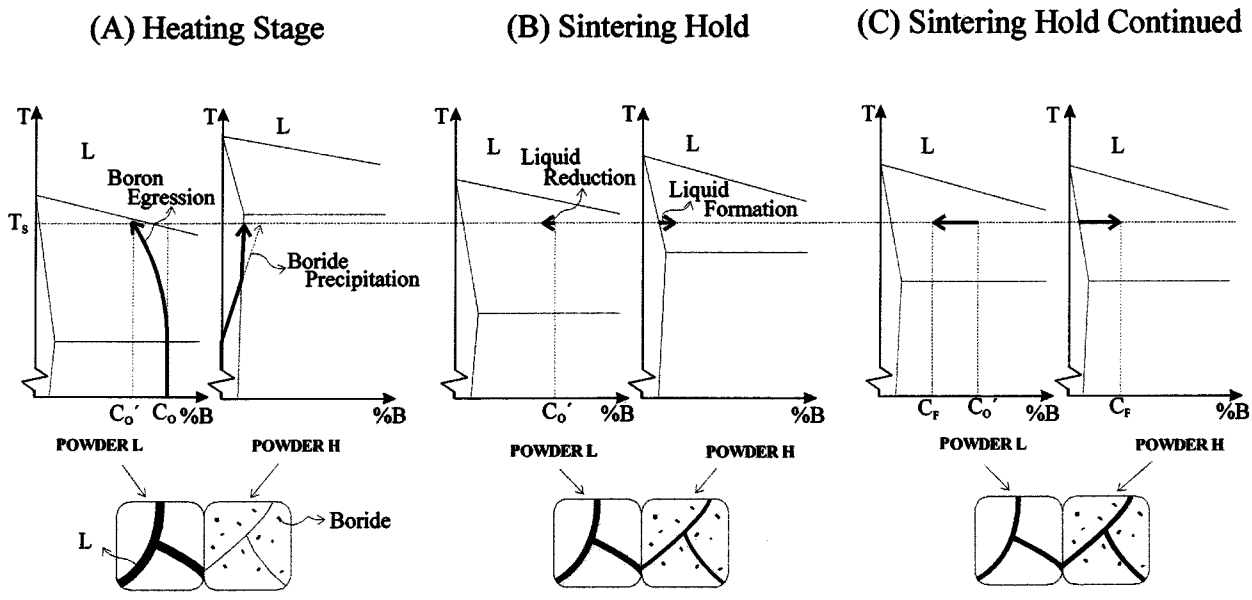

Figure 11 A schematic illustration of boron diffusion in mixtures of LM and HM powders, using separate hypothetical binary phase diagrams. T_S is the sintering temperature, C_0 is the initial boron content in the LM powder, C_0' is the boron content in the LM powder after boron precipitation in the HM powder, and C_F is the final equilibrium content in both the alloys. In each case, L denotes the liquid phase.

(refer to Fig. 11a). Further, the compositions of the two powders differ in other alloying elements to raise the eutectic temperature in the HM powder.

As the system is heated to the sintering temperature (T_S), liquid forms in the LM powder above its solidus temperature. Simultaneously, boron atoms diffuse into the adjacent HM particles. During heating, although the inherent HM powder is below the solidus temperature, boron diffusion generates boride precipitates in the particles. The solubility of boron in the HM matrix is negligible. Thus, at the beginning of the sintering hold, the boron content in the LM powder, designated C_0', is less than the initial content C_0 due to boron diffusion into the HM powder (as shown in Fig. 11a).

At the sintering temperature, boron continues to diffuse into the HM particles, reducing the liquid content in the LM powder (refer to Fig. 11b). The diffusing boron forms a eutectic liquid in the HM powder. Boride precipitates which form initially in HM powder are stable and do not dissolve in the liquid at the sintering temperature [23]. Simultaneously, interdiffusion of the other elements occurs, causing homogenization toward a mean composition (as manifested by the reduced gap between the eutectic temperatures for the two alloys).

Boron diffusion continues until the concentration is equal for particles of both the alloys (C_F), as shown in Fig. 11c. Boron diffusion is fast in comparison to the other alloying elements. The final weight fraction of boron in the system C_F dictates the equilibrium amount of liquid.

At temperatures lower than the LM liquidus, less liquid is formed on melting and the equilibrium concentration of boron in the liquid is high. For example, the concentration of boron in the liquid phase was 3.5 wt.% at 1080°C (refer to Table V) in comparison to 2.0 wt.% at 1145°C (refer to Table VII). Fig. 11 predicts that if the sintering temperature is only slightly higher than the eutectic temperature of the LM powder, then the HM powder will predominantly form borides. In fact, at 1080°C the HM powder formed borides with little liquid even after a 60 min hold (Fig. 4). The complex composition of the HM powder prevents the determination of the exact conditions which result in liquid formation rather than boride precipitation.

Gale and Wallach [30] obtained similar results for transient liquid phase bonding of Ni substrates using Ni-Si-B insert metals. At the onset of insert melting, boron diffused out of the liquid into the solid Ni substrate. If the temperature was below the Ni-B eutectic, then the diffusing boron formed precipitates (Ni_3B and $Ni_{23}B_6$) in the Ni substrate. At temperatures above the Ni-B eutectic, the diffusing boron caused localized liquation of the Ni substrates.

An increase in the sintering temperature and fraction of LM powder results in more liquid. High temperatures and high heating rates (where less time is spent at lower temperatures) decrease boride precipitation in the HM powder, leaving more boron available for liquid formation. Along with more liquid, higher temperatures also cause an exponential rise in diffusivity, leading to faster homogenization. A high peak temperature and high final boron content C_F (excluding the borides) result in excessive liquid in the final structures and formation of the script phase on cooling.

Transient liquid phase sintering is expected with such prealloyed powder mixtures [2]. The liquid formed on melting the LM powder disappears during sintering. A transient liquid has high solubility in the solid, with a final composition in a single-phase region at the sintering temperature [31–34]. However, transient liquid phase sintering does not appear feasible for the present system, since it requires complete solubility of the boron-rich liquid in the solid. There is almost negligible solid solubility of the HM powder in Ni [35]. Further, the solid present after a 60 min hold at 1145°C has no boron. Thus, boron diffusing into the HM powder forms either precipitates or liquid. Boron diffusion into the HM powder produces a eutectic liquid at temperatures above its solidus. Hence, the liquid is distributed throughout the compact (both LM and HM particles) and not just in the LM powder. With slow cooling, the liquid forms the script phase. If low quantities of LM powder are used, there is a possibility the liquid will disappear during isothermal sintering (especially if there is extensive boride precipitation). In that case, the densification and homogenization are slowed.

The current study may be extended to predict the behavior of other alloy systems. If the melting depressant has a higher solubility in the solid, then transient liquid phase sintering is possible. For example, Si may be used instead of B, as it has much higher solubility in the solid [35]. The diffusivity of Si in a Ni-based alloy is slower than boron,[‡] the various microstructural events associated with diffusion of the depressant into the high melting alloy are slower. Additionally, in case of the slower diffusing Si, grain boundary penetration of the liquid may be a mechanism for liquid formation in the high melting particles (as opposed to Si solid state diffusion into the high melting particles and subsequent liquation).

If the present system is used in brazing, then the diffusion of the melting depressant into the base-material must also be considered. This effect reduces the melting depressant content in the brazed region leading to isothermal solidification at the brazing temperature.

5. Conclusions

Microstructural evolution during the sintering of nickel-based prealloyed powder mixtures was followed.

1. Mixtures of powders of similar compositions may be sintered at temperatures above the solidus of the low-melt constituent to form a homogeneous and dense product.

2. Microstructural evolution reflects the chemical homogenization of the two constituent powders. The diffusion of the melting depressant, boron, from the

[‡] Kucera *et al*. [36] determined diffusivity at 1100°C for diffusion of boron and silicon out of a Ni-Cr-Si-B insert into nickel-based substrate (with Ti, Al, Fe, and Cr as major alloying elements) as 6.22×10^{-11} m^2 s^{-1} and 3.09×10^{-14} m^2 s^{-1}, respectively.

low-melt to the high-melt powder is the controlling feature.

3. Boron diffusion from the low-melt powder continuously increases its solidus temperature and results in incomplete melting even with peak temperatures above its liquidus. Boron diffusion can form either boride precipitates or liquid in the high-melt powder, depending on the temperature. During heating boron diffusion is responsible for both liquid formation and boride precipitation in the high-melt powder. There is simultaneous diffusion of other alloying elements, Ni, Co, Cr, Al, Ti, Ta, W, and Mo, between the two powders.

4. Hypothetical binary phase diagrams representing the two powders may be used to describe the interdiffusion mechanisms. An increase in temperature or the proportion of the low-melt powder increases the liquid content and promotes homogenization.

5. The boron-rich liquid is the precursor for precipitation of the compound script phase during slow cooling.

Acknowledgments

This research was funded by GE Aircraft Engines, Evendale, OH, and the National Science Foundation under grant DMR-9610280. Fruitful discussions with Drs. Anthony Griffo and T. S. Shivashankar are acknowledged.

References

1. R. M. GERMAN, *Metall. Mater. Trans. A* **28A** (1997) 1553.
2. R. TANDON and R. M. GERMAN, *Int. J. Powder Metall.* **30** (1994) 435.
3. R. M. GERMAN, "Liquid Phase Sintering" (Plenum Press, New York, NY, 1985).
4. B. E. MAGEE and J. LUND, *Z. Metallkd.* **67** (1976) 596.
5. K. TABESHFAR and G. A. CHADWICK, *Powder Metall.* **27** (1984) 19.
6. W. A. KAYSSER and G. PETZOW, *ibid.* **28** (1985) 145.
7. W. J. HUPPMANN and H. RIEGGER, *Inter. J. Powder Met. Powder Tech.* **13** (1977) 243.
8. S. FAROOQ and R. M. GERMAN, in Sintering '87, edited by S. Somiya, M. Shimada, M. Yoshimura and R. Watanabe (Elsevier Applied Science, London, 1988) Vol. 1, p. 459.
9. R. M. GERMAN, *Int. J. Powder Metall.* **26** (1990) 23 and 35.
10. S. R. BALA and J. A. LUND, *Z. Metallkd.* **70** (1979) 185.
11. J. A. LUND and S. R. BALA, in "Modern Developments in Powder Metallurgy, Vol. 6," edited by H. H. Hausner and W. E. Smith (Metal Powder Industries Federation, Princeton, NJ, 1974), p. 409.
12. J. A. LUND, R. G. BUTTERS and C. H. WEAVER, *Powder Met. Int.* **4** (1972) 173.
13. E. J. WESTERMAN, *Trans. TMS-AIME* **224** (1962) 159.
14. J. D. BOLTON and H. O. BAAH, *Powder Metall.* **24** (1991) 273.
15. R. H. PALMA, V. MARTINEZ and J. J. URCOLA, *ibid.* **32** (1989) 291.
16. C. S. WRIGHT, *ibid.* **32** (1989) 114.
17. S. LAL and G. S. UPADHYAYA, *Powder Met. Int.* **20** (1988) 35.
18. S. TALACCHIA, J. AMADOR and J. J. URCOLA, *Metal Pow. Rep.* **50** (1995) 16.
19. E. LUGSCHEIDER, V. DIETRICH and J. MITTENDORFF, *Welding J.* **67** (1988) 47s.
20. E. LUGSCHEIDER, T. SCHITTNY and E. HALMOY, *ibid.* **68** (1989) 9s.
21. J. W. CHASTEEN and G. E. METZGER, *ibid.* **58** (1979) 111s.
22. S. K. TUNG and L. C. LIN, *Mater. Sci. Technol.* **10** (1994) 364.
23. R. G. IACOCCA, *Metall. Mater. Trans. A* **27A** (1996) 145.
24. A. LAL, R. G. IACOCCA and R. M. GERMAN, *ibid.* **30A** (1999) 2201.
25. *Idem.*, "Advances in Powder Metallurgy and Particulate Materials-1996, Vol. 3," (Metal Powder Industries Federation, Princeton, NJ, 1996), p. 11.289.
26. P. J. MCGINN, A. E. MILLER, P. KUMAR and A. J. HICKL, in "Progress in Powder Metallurgy, Vol. 38," edited by J. G. Bewley and S. W. McGee (Metal Powder Industries Federation, Princeton, NJ, 1982) p. 449.
27. P. F. MURLEY and R. M. GERMAN, in "Advances in Powder Metallurgy, Vol. 3," compiled by T. G. Gasbarre and W. F. Jandeska (Metal Powder Industries Federation /APMI International, Princeton, NJ, 1989) p. 103.
28. A. LAL, M.S. thesis, The Pennsylvania State University, University Park, PA, December 1996.
29. C. T. SIMS, N. S. STOLOFF and W. C. HAGEL, in "Superalloys II, edited by C. T. Sims, N. S. Stoloff, and W. C. Hagel (Wiley, New York, NY, 1987) p. 97.
30. W. F. GALE and E. R. WALLACH, *Metall. Trans. A*, **22A**, (1991) 2451.
31. R. M. GERMAN and J. W. DUNLAP, *ibid.* **17A** (1986) 205.
32. D. J. LEE and R. M. GERMAN, *Inter. J. Powder Met.* **21** (1985) 9.
33. J. PUCKERT, W. A. KAYSSER and G. PETZOW, *Inter. J. Powder Met. Powder Tech.* **20** (1984) 301.
34. R. M. GERMAN, "Sintering Theory and Practice" (Wiley-Interscience, New York, NY, 1996) p. 391.
35. T. B. MASSALSKI (Ed.), "Binary Alloy Phase Diagrams," 2nd ed. (American Society for Metals, Metal Park, Ohio, 1986.)
36. J. KUCERA, A. BUCHAL, A. REK and K. STRANSKY, *Kovove Mater.* **22** (1984) 250.

Received 8 November 1999
and accepted 9 March 2000